Two-photon double ionization of helium: An experimental lower bound of the total cross section

Philippe Antoine, Emmanuel Foumouo, and Bernard Piraux
Unité de Physique Atomique, Moléculaire et Optique Université catholique de Louvain, Chemin du Cyclotron, 2 B-1348 Louvain-la-Neuve, Belgium

Toshihiko Shimizu, Hirokazu Hasegawa, Yasuo Nabekawa, and Katsumi Midorikawa
Laser Technology Laboratory, RIKEN, 2-1 Hirosawa, Wako-shi, Saitama, 351-0198, Japan
(Received 24 April 2008; revised manuscript received 30 June 2008; published 22 August 2008)

We report on the experimental estimation of a lower bound of helium. Our experiment differs from a previous one described by Hasegawa *et al.* [Phys. Rev. A **71**, 023407 (2005)]. The photons that correspond to the 27th harmonic of a Ti:sapphire laser have an energy of 41.8 eV. The extraction of the cross section rests on a theoretical model, based on the rate equations, that fully includes the contribution from the sequential channels and the macroscopic effects. Some of the experimental parameters are very difficult to measure accurately. For those parameters, we deliberately consider values compatible with their experimental determinations and that lead systematically to an underestimation of the two-photon double ionization cross section. Our estimation of this lower bound is higher than a bunch of various theoretical results. It stays, however, too close to these latter ones to draw any definite conclusion about their validity, even though it clearly indicates that the actual value of the double ionization cross section is higher than expected.

DOI: 10.1103/PhysRevA.78.023415 PACS number(s): 32.80.Rm, 32.80.Fb, 42.50.Hz, 42.65.Ky

I. INTRODUCTION

In the xuv regime, few-photon double ionization of atoms or molecules is a fundamental problem which is far from being understood. From the experimental point of view the main activity has concentrated until recently on one-photon processes with synchrotron radiation. Moving from one-photon processes to two-photon processes requires higher intensities that are at the edge of the current technologies. Preliminary experiments with high-order harmonic generation [1] and with free electron radiation [2] have been performed but it is too premature to draw any definite conclusions on the validity of the predictions of the existing theoretical models [3–11]. In addition, there is no consensus between these predictions. There are differences of more than one order of magnitude on the total cross section. The existence of such discrepancies contrasts with the perfect agreement for one-photon double ionization between the experimental data and the predictions of the same theoretical approaches. It is worth noting that all are based on some approximations. The lack of consensus for theoretical two-photon double ionization (TPDI) cross section seems to suggest that the double escape mechanism differs from that of one-photon double ejection. In particular, the role of the final state electron correlation has been pointed out by Foumouo *et al.* [12] who has recently proposed a mechanism of double ejection.

In this contribution, we present a measurement of the lower bound of the TPDI cross section. This cross section estimation is based on the ratio of the single ionization yield to the double ionization yield. This method is much less sensitive to laser parameters and pressure than our previous results [1]. The data analysis includes a full description of the laser beam and takes into account the sequential channels. In particular, the impact of the single ionization-excitation (of the residual ion) channels is discussed and shown to have an important role when extracting the TPDI yield from the total double ionization yield.

The manuscript is organized as follows. Section II includes a short description of our TPDI theoretical model. The experiment is presented in Sec. III. Finally the last section is devoted to the calculation performed to extract the TPDI cross section and to the interpretation of the experimental data. The section concludes with a comparison with the previous experimental results and the different theoretical predictions.

II. THEORY

Our computational treatment of the two-photon double ionization cross section rests on the solution of the time-dependent Schrödinger equation (TDSE)

$$i\frac{\partial}{\partial t}\Psi(\mathbf{r}_1,\mathbf{r}_2,t)=\left[-\frac{1}{2}\nabla_{r_1}^2-\frac{1}{2}\nabla_{r_2}^2-\frac{Z}{r_1}-\frac{Z}{r_2}+\frac{1}{r_{12}}+D_G(t)\right]\times\Psi(\mathbf{r}_1,\mathbf{r}_2,t). \quad (1)$$

Z denotes the charge of the nucleus ($Z=2$ for He), which is assumed to be infinitely massive. $\mathbf{r}_1$ and $\mathbf{r}_2$ are the radial coordinates of both electrons and $r_{12}=|\mathbf{r}_1-\mathbf{r}_2|$ is the inter-electronic distance. $D_G(t)$ describes the dipole interaction of the system with the oscillating field either in the length gauge ($G\equiv L$) or in the velocity gauge ($G\equiv V$):

$$D_L(t)=\mathbf{E}(t)(\mathbf{r}_1+\mathbf{r}_2), \quad (2)$$

$$D_V(t)=-i\mathbf{A}(t)(\boldsymbol{\nabla}_1+\boldsymbol{\nabla}_2). \quad (3)$$

$\mathbf{E}(t)$ denotes the electric field and $\mathbf{A}(t)=\hat{z}A_0f(t)\sin(\omega t)$ the corresponding vector potential which oscillates at the frequency ω and which is assumed linearly polarized along the z axis. $f(t)$ is the pulse envelope given by

$$f(t)=\cos^2(t/\tau),\quad |t|\leqslant\pi\frac{\tau}{2},$$

$$=0, \quad |t| > \pi\frac{\tau}{2}. \tag{4}$$

The method to solve Eq. (1) has been described in great details in Ref. [7]. In short, we expand the full wavepacket of the system $\Psi(\mathbf{r}_1,\mathbf{r}_2,t)$ in terms of its field-free eigenstates. The wave functions associated with these eigenstates are calculated within a spectral method that consists of diagonalizing the atomic Hamiltonian in a basis of products of Coulomb Sturmian functions of the electron radial coordinates and bipolar harmonics of the angular coordinates. The full wavepacket of the system is then time propagated by means of an explicit Runge-Kutta method. In order to calculate the probabilities of single and double ionization, we proceed as follows. By using the Jacobi-matrix method, we generate a multichannel scattering wave function associated with a given single ionization channel. At the end of the interaction with the external field, we project the final electron wavepacket on this scattering wave function and sum over all single ionization channels. We obtain in this way, the single ionization probabilities. The double ionization probability is evaluated by subtracting the probability for single escape from the total ionization probability. Note that the total ionization probability does not require the knowledge of the asymptotic conditions. It is simply obtained as one minus the probability to be in a bound state of helium at the end of the interaction with the pulse. Our estimate of the N-photon double ionization (generalized) cross sections σ_N is based on the following relation between the N-photon transition probability P_N and σ_N:

$$P_N = \sigma_N \int_{-\infty}^{\infty} dt \Phi^N(t), \tag{5}$$

where Φ is the photon flux. In the present case, pulse durations of ten optical periods are sufficient to ensure the stability of σ_N. We have checked that our estimate of the cross sections is converged with respect to the basis size and is gauge independent. In addition, our results for the total one-photon single and double ionization cross sections are in very good agreement with those obtained with more sophisticated theories both in the case of He and H^- [7].

Before considering the TPDI process, let us examine the two-photon single ionization (TPSI) (with excitation of the residual ion) of He. Within the present context, the estimate of the corresponding cross sections is necessary to evaluate the weight of the following sequential three-photon processes:

$$\mathrm{He} + \hbar\omega \rightarrow \mathrm{He}^+(1s) + 2\hbar\omega \rightarrow \mathrm{He}^{2+}, \tag{6a}$$

$$\mathrm{He} + 2\hbar\omega \rightarrow \mathrm{He}^{+*} + \hbar\omega \rightarrow \mathrm{He}^{2+}, \tag{6b}$$

that contribute to the double ionization yield. While the first one [process (6a)] has been extensively discussed in the litterature (see, for example, Ref. [13]) the second one [process (6b)] has often been neglected. If TPSI of helium does not involve any relaxation of the residual ion before the second photon is absorbed, these two-photon transitions are direct as illustrated by processes 3 and 4 of Fig. 1. Note that these processes cannot occur without electron correlation. Direct TPSI corresponds to the first step of the second sequential process. It should not be confused with the so-called above threshold ionization (ATI) process in which the residual ion is left in its ground state after the absorption by one electron of more than the minimum number of photons needed for single ionization (one photon in the present case) (process 2 in Fig. 1). ATI does not require electron correlation. In the present context ATI process is safely neglected because single ionization of helium is by far, dominated by the one-photon process. TPSI of helium may also occur sequentially: after absorbing one photon, the residual ion He^+ relaxes into its ground state and is then excited into a np state following the absorption of the second photon (process 1 in Fig. 1) In that case, the process can be resonant at frequencies that correspond to the $1s$-np transitions of the core He^+. Formally, sequential TPSI is part of the first sequential three-photon double ionization of helium [process (6a)].

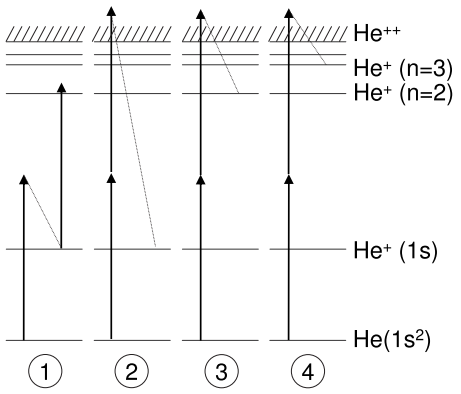

FIG. 1. Energy diagram of He, He^+, and He^{2+} and dominant single ionization channels: (1) sequential two-photon single ionization (TPSI), (2) above threshold ionization (ATI), (3 and 4) direct TPSI.

One of the drawbacks of all time-dependent approaches is the impossibility of separating the direct and the sequential processes. Because in the present case, sequential TPDI can be resonant, it is expected to dominate the direct TPSI process. As a result, it becomes impossible to accurately evaluate the direct TPSI cross section within any time-dependent approach. This point is illustrated in Fig. 2 where we show the TPSI total and partial cross sections, calculated within our time-dependent approach, as a function of the pulse duration at a frequency corresponding to the first core resonance ($1s$-$2p$ transition of He^+). The fast increase of these cross sections with the pulse duration is a clear indication that the two-photon sequential process dominates. Note that at very low field intensity and not too close to resonance, the sequential TPSI probability varies quadratically with the pulse duration. In these conditions, the notion of cross section loses its meaning.

The estimation of the direct TPSI cross section has to be based on the calculation of the probability amplitude with a time-independent approach. The best candidate is probably the lowest nonvanishing order of perturbation theory. Nakajima and Nikolopoulos computed the direct TPSI cross section but only at a photon energy of 45 eV [14]. Later on,

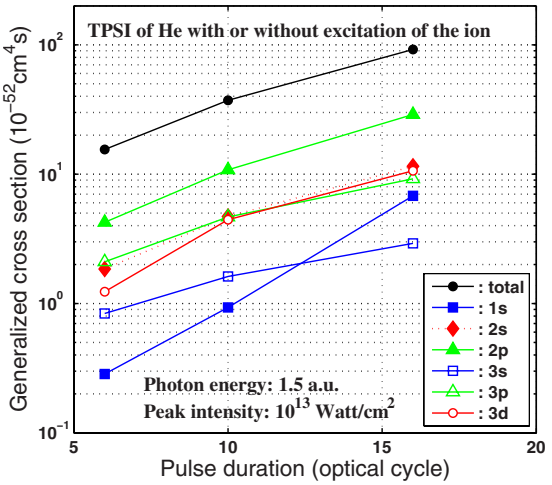

FIG. 2. (Color online) Total and partial cross sections for TPSI of He as a function of the pulse duration used in our time-dependent approach. The photon energy is equal to 1.5 a.u. which corresponds to the $1s$-$2p$ core resonance. The peak intensity of the pulse is 10^{13} W/cm^2. The partial cross sections with the residual ion left in the $1s$, $2s$, $3s$, $2p$, $3p$, or $3d$ are considered.

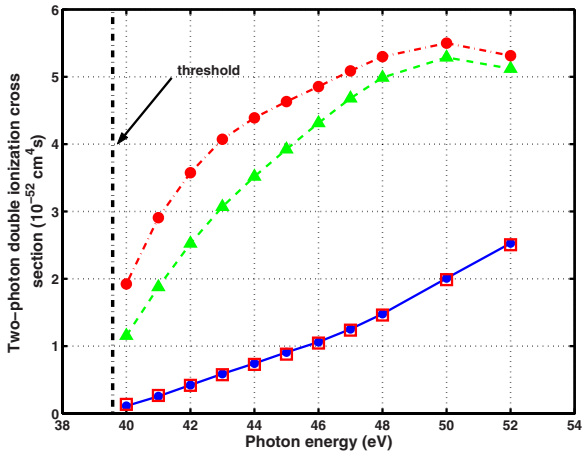

FIG. 3. (Color online) Total cross section for TPDI of He. The dot-dashed curve is our fully correlated result obtained within the Jacobi-matrix method. The full curve is our result obtained by projecting the final wavepacket onto a product of two Coulomb functions. The squares that are on the full curve are obtained by "switching off" the Coulomb repulsion in the single continuum wave function generated by the Jacobi-matrix method. The full triangles are obtained by taking into account the radial correlations in the single continuum wave function generated by the Jacobi-matrix method.

Feng and van der Hart [4] with their R-matrix Floquet approach and Shakeshaft [10] with a generalization of the flux formula obtained results that are in good agreement over a wide frequency range and also very close to an estimation of Lambropoulos at the frequency of the present experiment [15]. Quite unexpectedly, the results of Feng and van der Hart and of Shakeshaft exhibit a very strong resonant behavior around the $1s$-np transition frequencies of He^+. The interpretation of these results remains unclear and in particular the fact that the first of these core resonances ($1s$-$2p$) has a very strong impact over a wide range of photon energies. Upon this condition, we consider these data as an overestimation of the actual direct TPSI cross section when analyzing the raw experimental measurements.

In Fig. 3, we present our results for the TPDI cross section. If we subtract the single ionization probabilities, evaluated by means of the Jacobi-matrix method, from the total ionization probability and use the adiabatic approximation to extract the corresponding cross section, we obtain the upper dot-dashed curve. On the other hand, if we project directly the final wavepacket on a noncorrelated final state, namely, a product of two Coulomb wave functions, we obtain the lower full curve. The large difference between the two curves already indicates that the final state correlation plays a crucial role. In order to gain more insight, let us go back to our Jacobi-matrix calculations and let us "switch off" the electron correlations in the single continuum wave function. By means of the same subtraction procedure, we get, as expected, a TPDI cross section (squares) that coincides exactly with the results obtained by projecting the final wavepacket on a product of two Coulomb wave functions. Furthermore, if, in our Jacobi-matrix calculation of the single continuum wave function, we keep only the radial correlations, we obtain a TPDI cross section (dashed curve with triangles) which is very close to our fully correlated results. In other words, it is the radial coupling between various ionization channels that is responsible for the strong effect we observe in the TPDI cross section. This conclusion is consistent with the TPDI mechanism we proposed in a recent paper [12] in which we show that the angular correlations force both electrons to escape back-to-back along the polarization axis while the dynamical screening (radial correlations) leads to an equipartition of the electron energy.

III. THE EXPERIMENT

We have already reported in Refs. [1,16,17] on the production of He^{2+} resulting from the interaction of He with the intense 27th harmonic pulse of a femtosecond Ti:sapphire laser. Our analysis for extracting the TPDI cross section from experimental data was based on the estimation of the absolute number of ions from the measured time-of-flight (TOF) spectra of ions. The estimated TPDI cross section was in relatively good agreement with all the theoretical predictions within the uncertainty of the experimental conditions. We can notably mention the efficiency of the ion detector, the determination of the atomic density in the interaction region with the laser. Furthermore, the intensity of the laser field can be affected by fluctuations in pulse energy, pulse duration, and beam diameter at the focal point.

The present contribution concerns a new measurement but with a similar setup. The main difference is the experimental parameter that is used for the TPDI cross section estimation. Previously it was based on the absolute number of He^{2+} ions while here, the input data is the ratio of the number of He^{2+} ions (N^{2+}) to that of He^+ ions (N^+). The advantage is twofold. First this ratio is independent of the atomic density, at least when the single ionization yield does not saturate. Second, it depends on the ratio of the detection efficiencies for He^+ and

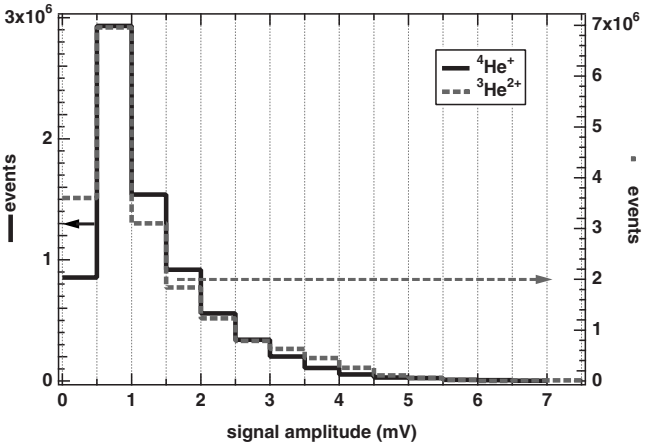

FIG. 4. Histograms of signal heights for He^+ (solid line) and He^{2+} (dashed line).

He^{2+}, respectively. This is much less sensitive than the detection efficiency itself. In our experimental conditions we assume that the detection efficiency ratio is equal to 1. This is motivated by the two following observations. A first indication comes from the signal height distributions that are plotted in Fig. 4. The distributions for He^+ and He^{2+} look very similar. They are approximated by Poisson distributions with parameters equal to 2.6 and 2.3 for He^+ and He^{2+}, respectively. The Poisson parameter is linked to the mean number of electrons created at the impact of an ion. This suggests that the probability to generate no electron at the impact of an ion is low for both ions. As such, the detection efficiencies for He^+ and He^{2+} are quite close. Secondly, we interpret the traces of the TOF spectra in a counting mode instead of an averaging mode. More precisely we count the number of signals that exceed a given threshold. We repeat the counting for He^+ and He^{2+} and compute the ratio of the two counts. It is worth noting that the two methods (signal averaging and counting) give two estimations of the ion ratio that differ by roughly 10% only. Practically we obtain the ion number ratio by simply calculating the ratio of the amounts of electrical signals in the TOF mass spectra without regarding the absolute number of each ion.

The setup shown in Figs. 5 and 6 is similar to that used in previous experiments [1,16,17]. Pump laser pulses are delivered by a chirped pulse amplification (CPA) system of a Ti:sapphire laser with a repetition rate of 10 Hz. The mean pulse energy is 20 mJ. The laser beam is focused using a positive lens with a focal length of 5 m. A 10 cm gas cell is filled with argon. The focal position of the fundamental laser field and the gas pressure of the argon are adjusted as such to maximize the harmonic production [18,19]. An harmonic-separator mirror made of silicon replaces the silicon carbide mirror that was used in our previous experiment in order to reflect the harmonic beam into the TOF chamber for ion spectroscopy.

The silicon harmonic-separator mirror [20] achieves a higher extinction ratio of the harmonic beam to the fundamental laser beam. The lower damage threshold of this mirror is compensated by placing the separator mirror farther from the gas cell for high-order harmonic generation, thereby increasing the beam diameters of both the fundamental laser and the high-order harmonic beams. The reflectivity of the harmonic-separator mirror for the linear *p*-polarized fundamental laser beam is estimated to be less than 10^{-4} due to the nature of the Brewster incidence of the laser beam, while that for the harmonic beam exceeds 40% in the wavelength range from 26–40 nm [19,20]. The undesired edge of reflected harmonic fields from the harmonic separator mirror is truncated with an aperture. The diameter of the aperture is increased from 3 to 5 mm to be adapted to the increased beam diameter of the harmonic beam. The harmonic beam passes 5 mm below the entrance hole of the acceleration plates for the ions in the TOF chamber. The spherical concave mirror with a multilayer SiC/Mg coating reflects almost only the 27th-order harmonic beam with a reflectivity of 24% [1]. The beam is focused with a focal length of 50 mm in front of the entrance hole of the TOF spectrometer.

Its diameter is 1 mm. We have adopted this off-axis configuration to prevent the microchannel plates (MCPs) from detecting ions created from one-photon absorption of the unfocused harmonic beam. Ion signals are sent to a digital oscilloscope with a bandwidth of 500 MHz (Lecroy, LT374L) and recorded in a computer. The target helium gas is supplied through a variable leak valve, instead of a pulsed gas valve. So the helium statically fills the chamber resulting in an uniform pressure. This fixes the problem of the determination of the atomic density in the interaction region observed in our previous experiments [1,16,17].

An important issue when determining the N^{2+}/N^+ ratio is the possible saturation of the He^+ yield. The electrical signals from a MCP may saturate when two or more ions simultaneously hit a channel in the MCP. We have checked the linearity of the N^+ signal ($^4He^+$ yield) by tuning the ^4He static pressure. In Fig. 7, the $^4He^+$ signal area averaged over 1000 TOF mass spectra is plotted against the pressure. Note that the pressure is the value read on the ion gauge. The

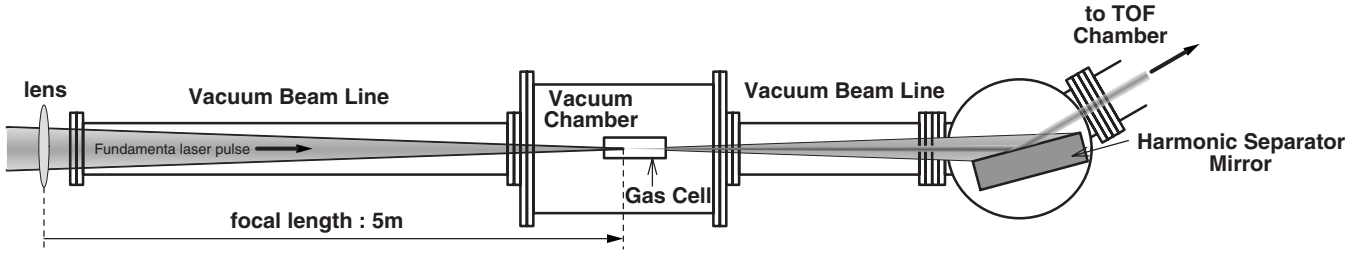

FIG. 5. Schematic view of the experimental setup for high-order harmonic generation. Details of the harmonic generation are given in Refs. [18,19].

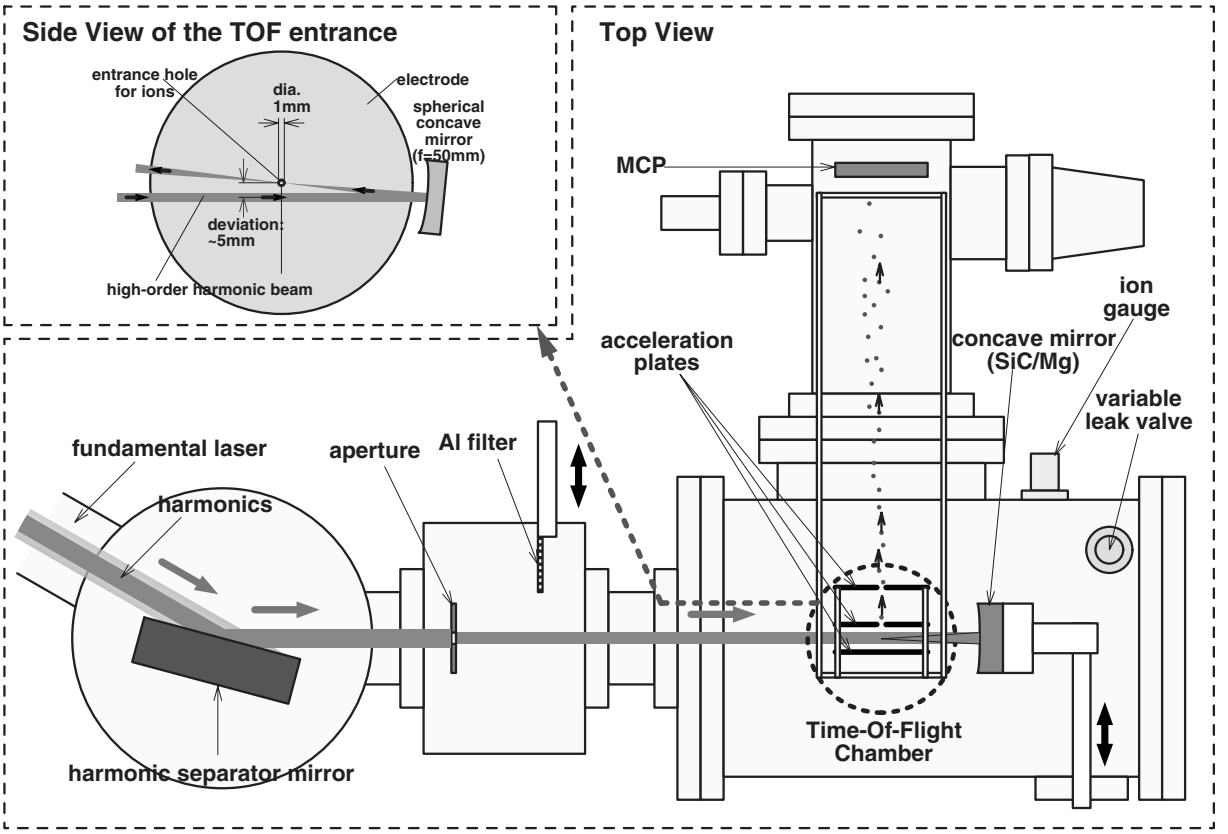

FIG. 6. Top view of the time-of-flight spectrometer and optics. Enlarged side view of the configuration for the TOF entrance hole is also shown in the inset.

calibrated pressure of ^{4}He or ^{3}He is obtained by dividing by a factor (0.18).

The pressure dependence of the signal is linear only for low pressure. Above 2×10^{-6} Torr saturation is observed. Nevertheless we are forced to operate at high pressure even if saturation is not negligible because the double ionization yield is very low. Saturation is corrected by extrapolating the linear pressure dependence into the pressure range that exhibits saturation (pressure $>2\times10^{-6}$ Torr). The straight line in Fig. 7 represents the single ionization yield corrected for saturation.

We use the ^{3}He isotope, instead of ^{4}He, in order to eliminate the H_2^+ signal at $m/z=2$ that originates from water molecules contained as an impurity in the TOF chamber. The TOF mass spectrum ranging from $m/z=1$ to 2 is shown in Fig. 8. It is an average over 6000 traces. The ^{3}He pressure is maintained at $(1.37\pm0.08)\times10^{-4}$ Torr during all the measurements. From the measured spectrum at $m/z=1.5$, the signal areas corresponding to $^3He^{2+}$ and $^3He^+$ are evaluated to be equal to 0.47 pV s and 10 ± 0.6 nV s, respectively. This latter value includes the saturation correction. From these

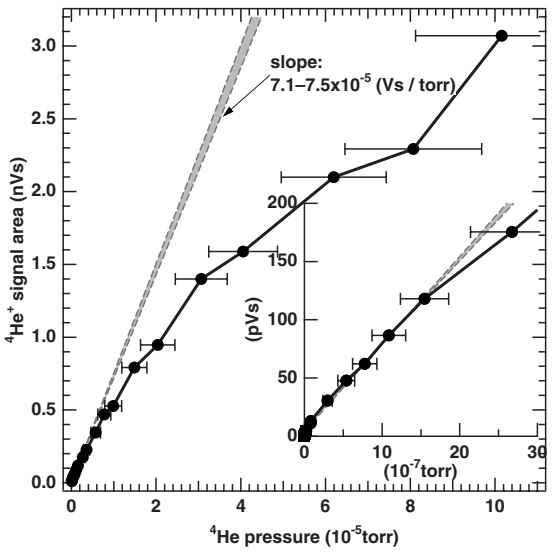

FIG. 7. $^4He^+$ signal area of TOF mass spectrum against ^{4}He atomic pressure read on the ion gauge. Magnified plot at low pressures is shown in the inset.

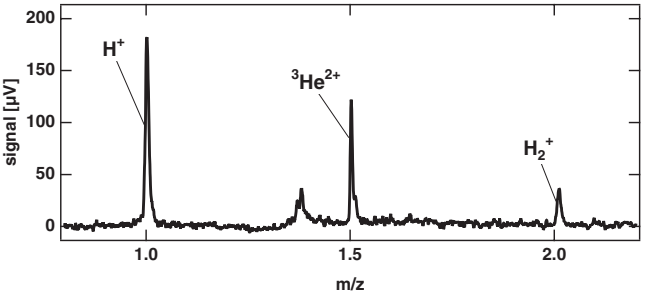

FIG. 8. TOF mass spectrum with ^{3}He gas. The H^+ and H_2^+ peaks are due to impurities.

figures, we conclude that the N^{2+}/N^{+} ratio is equal to $(4.7 \pm 0.3) \times 10^{-5}$. It is worth noting that the ratio depends on the focusing geometry (see Sec. IV).

The pulse energy of the 27th-harmonic beam U is computed by multiplying the pulse energy (320 nJ) at the exit of the gas cell [18] by the reflectivity of each optical element [0.45 (reflectivity of the silicon harmonicseparator mirror [20]) $\times 0.7$ (throughput of the aperture [17]) $\times 0.24$ (reflectivity of the concave mirror [16])]. As such, the pulse energy in the interaction region is estimated to be 24 nJ.

The full width at half maximum (FWHM) of the autocorrelation trace of the 27th-harmonic pulse is measured to be 11 fs. So the pulse width τ is estimated to be 10 fs [17]. We come back to the exact definition of τ in the next section.

The beam radius at e^{-2} of the maximum in the focal plane, noted w_0, is estimated to be 1.5 μm or larger. The M^2 of the harmonic beam is ~ 1.4 [19,21].

The peak intensity I_0 is calculated from $U/(\tau \pi w_0^2/2)$, to be 6.8×10^{13} W/cm^2. The estimated I_0 is the upper limit of the actual intensity applied to the experiment, because the degradation of the optics and the deviation from the ideal focusing condition always reduce I_0. In fact, we have observed that the reflectivity of the concave mirror decreases with long time use. A reduction of the reflectivity of SiC/Mg coating from 38 to 15 % has been reported in the past. Astigmatism inevitably accompanies the off-axis configuration of the concave mirror. It might result in an increase of 10% of the beam diameter.

IV. INTERPRETATION

In the present experiment the laser peak intensity is as high as 6.8×10^{13} W/cm^2 but this is still in the perturbative regime as $U_p/h\nu \approx 1.3 \times 10^{-4} \ll 1$, where U_p is the ponderomotive potential. In such a condition, all the transitions relevant for double ionization are characterized by a transition rate that is linearly or quadratically proportional to the intensity depending on the number of photons involved. Such a formalism is applicable in the present case even in the presence of the $1s$-$2p$ resonance of the He^+ ion since the laser bandwidth (FWHM=0.18 eV) is small with respect to the gap between the photon energy and the resonance (1 eV). Moreover only the processes involving the minimum number of photons have to be considered. Here we restrict the study to the photon energy range between the TPDI threshold (39.5 eV) and the one-photon ionization of $He^+(1s)$ (54.4 eV). So the dominant channels are the two-photon direct double ionization and the three-photon sequential double ionization. Two different sequential processes are considered depending on the intermediate state, namely, the ground state [Eq. (6a)] or an excited state of the ion [Eq. (6b)]. The $He^+(1s)$ ion can be created by absorption of a single photon but two additional photons are necessary to reach the double continuum. In contrast, two photons are necessary to leave the He^+ ion in an excited state but a single additional photon is sufficient to produce He^{2+} ions. The different channels are illustrated in Fig. 9. As stated, the rates for all the relevant transitions can be expressed as

$$\Gamma_{\mathrm{dir}}^{2+} = \sigma_{\mathrm{dir}}^{2+} (I/h\nu)^2, \tag{7a}$$

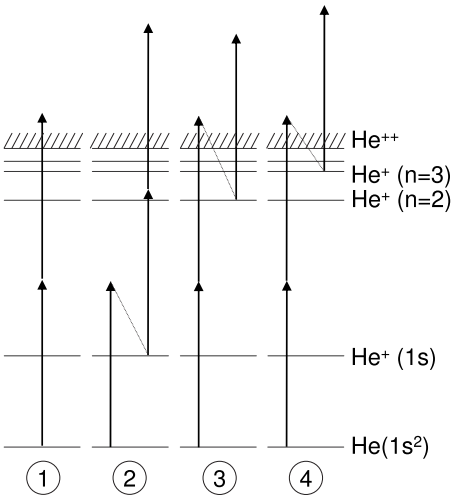

FIG. 9. Energy diagram of He, He^+, and He^{2+} and dominant double ionization channels: (1) TPDI, (2) three-photon sequential process 6*a*, (3 and 4) three-photon sequential process 6*b*.

$$\Gamma_{\mathrm{seq}_1}^{+} = \sigma_{\mathrm{seq}_1}^{+} (I/h\nu), \tag{7b}$$

$$\Gamma_{\mathrm{seq}_{2_n}}^{+} = \sigma_{\mathrm{seq}_{2_n}}^{+} (I/h\nu)^2, \tag{7c}$$

$$\Gamma_{\mathrm{seq}_1}^{2+} = \sigma_{\mathrm{seq}_1}^{2+} (I/h\nu)^2, \tag{7d}$$

$$\Gamma_{\mathrm{seq}_{2_n}}^{2+} = \sigma_{\mathrm{seq}_{2_n}}^{2+} (I/h\nu). \tag{7e}$$

The time evolution of the populations is driven by the rate equations (8). The sum over the excited states of the He^+ ion states formally includes all the He^+ states excepted the ground state. The P^0, $P_{\mathrm{seq}_1}^{+}$, $P_{\mathrm{seq}_{2_n}}^{+}$ are the populations of the He ground state, the He^+ ground state and the $He^+(n)$ excited state, respectively. The populations of the double continuum are labeled P_{dir}^{2+}, $P_{\mathrm{seq}_1}^{2+}$ and $P_{\mathrm{seq}_2}^{2+}$ according to the ionization process: direct process, sequential process 1 [see process (6a)], and sequential process 2 [see process (6b)], respectively,

$$\frac{dP^0}{dt} = \left(-\Gamma_{\mathrm{dir}}^{2+} - \Gamma_{\mathrm{seq}_1}^{+} - \sum_i \Gamma_{\mathrm{seq}_{2_i}}^{+} \right) \times P^0, \tag{8a}$$

$$\frac{dP_{\mathrm{seq}_1}^{+}}{dt} = \Gamma_{\mathrm{seq}_1}^{+} \times P^0 - \Gamma_{\mathrm{seq}_1}^{2+} \times P_{\mathrm{seq}_1}^{+}, \tag{8b}$$

$$\frac{dP_{\mathrm{seq}_{2_n}}^{+}}{dt} = \Gamma_{\mathrm{seq}_{2_n}}^{+} \times P^0 - \Gamma_{\mathrm{seq}_{2_n}}^{2+} \times P_{\mathrm{seq}_{2_n}}^{+}, \tag{8c}$$

$$\frac{dP_{\mathrm{dir}}^{2+}}{dt} = \Gamma_{\mathrm{dir}}^{2+} \times P^0, \tag{8d}$$

$$\frac{dP_{\mathrm{seq}_1}^{2+}}{dt} = \Gamma_{\mathrm{seq}_1}^{2+} \times P_{\mathrm{seq}_1}^{+}, \tag{8e}$$

TABLE I. One-photon single ionization cross section of He at 41.8 eV.

Authors	σ (in 10^{-18} cm^2)
Nikolopoulos *et al.* [22]	2.77
Samson *et al.* [23]	2.86
This work	2.92

$$\frac{dP^{2+}_{\mathrm{seq}_2}}{dt} = \sum_i \Gamma^{2+}_{\mathrm{seq}_{2_i}} \times P^{+}_{\mathrm{seq}_{2_i}}. \tag{8f}$$

The good agreement between cross sections characterizing the sequential channel via the $He^+(1s)$ state (see Tables I and II) suggests that the theoretical values can be trusted when estimating the corresponding ionization yields. Our cross section of the two-photon ionization of $He^+(1s)$ is slightly higher than that of Nikolopoulos *et al.* [22] but this is without any consequence as we aim at estimating a lower bound of the TPDI cross section. Our results are plotted in Fig. 10. It is worth noting that the pulse duration in our simulation of this sequential channel is very close to that of the experiment in order to correctly describe the $1s$-$2p$ resonance.

The description of sequential channel via the excited states with the time-dependent model is problematic because it requires a pulse duration as long as 100 cycles due to the presence of the $1s$-$2p$ core resonance (see discussion in Sec. II). Unfortunately this is numerically untractable so far. In these conditions we use cross sections estimated by a time-independent model [25]. This should be an appropriate model as the experimental parameters correspond reasonably to an off-resonance condition. It is worth noting that the possible small error introduced by using cross sections estimated by a time-independent model leads to an overestimation of the sequential ionization yield and so it will push the lower bound of the TPDI cross section slightly down. The TPSI cross sections of He are plotted in Fig. 11 for the residual He^+ ion in the first excited states.

In a perturbative regime and when population depletion is negligible, the double ionization yield from a particular sequential channel is directly proportional to the product of the cross sections that characterize the one-photon step and the two-photon step. These products of cross sections for the sequential processes via the first states of He^+ are plotted in Fig. 12 for 41.8 and 44.9 eV photon energy, respectively. These energies correspond to the 27th and 29th harmonics of a Ti:sapphire laser, respectively. The following comments can be drawn from Figs. 11 and 12. The single ionization-

TABLE II. Two-photon ionization cross section of at He^+ at 41.8 eV.

Authors	σ (in 10^{-52} cm^4 s)
Nikolopoulos *et al.* [22]	1.8
Chan *et al.* [24]	2.9
This work	2.74

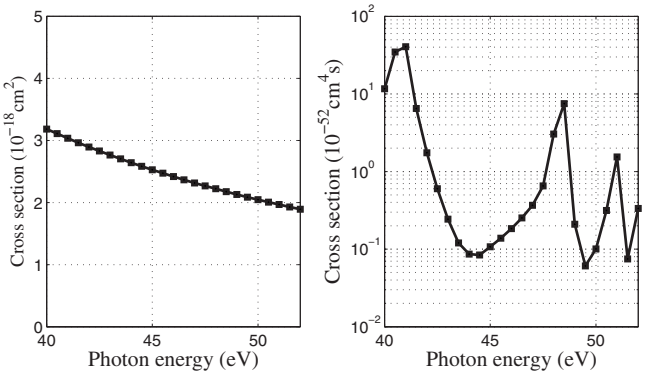

FIG. 10. Cross sections involved in the sequential channel ($6a$) computed with a time-dependent model: (a) cross section of the one-photon ionization of, (b) cross section of the two-photon ionization of $He^+(1s)$.

excitation channels significantly affect the sequential processes. As shown in Fig. 11, only the single ionization with excitation into the $2p$ state of He^+ plays a role in the context of the present experiment. Above 46 eV the contribution of the $3p$ states becomes more important because the photon energy is closer to $1s$-$3p$ resonance of He^+. As pointed out by Nikolopoulos *et al.* [13] the most appropriate photon energy for a TPDI experiment is the one corresponding to the 29th harmonic as it would reduce the sequential ionization yield by more than one order of magnitude. From Fig. 12, we see that the contributions from the two sequential processes are of the same order when using TPSI cross section calculated by the time-independent approach [4,25].

By solving the set of differential equations, we accurately describe the dynamics of the double ionization process in the perturbative intensity range. For example, this approach includes competition between the direct process and the sequential channels, depletion of the initial state $He(1s^2)$ and influence of the time profile of the laser pulse. Moreover by averaging the ionization yield over the spatial laser intensity distribution, we get the macroscopic ionization yields of the different channels. Only these spatially and temporally averaged yields can be compared with experimental results.

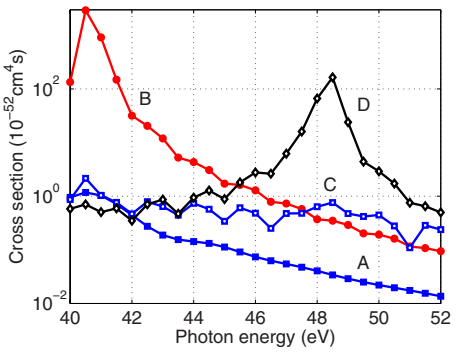

FIG. 11. (Color online) TPSI cross sections of He computed with a time-independent model [25] for various final states: $2s$ (filled blue squares, A label), $2p_0$ (filled red circles, B label), $3s$ (open blue squares, C label), and $3p_0$ (open black diamonds, D label). The cross section to the $2p_{\pm 1}$ state is not plotted because it coincides almost with that to the $2p_0$ state.

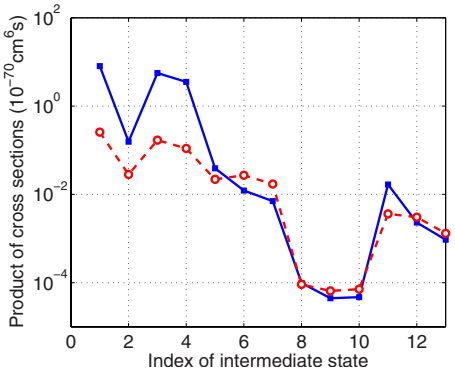

FIG. 12. (Color online) Products of the cross sections of the one-photon step and the two-photon step of the sequential processes. The channel indexes refer to the intermediate state. It corresponds to the $1s$ (sequential process 1 [see Eq. (6a)]), $2s$, $2p_0$, $2p_1$, $3s$, $3p_0$, $3p_{\pm 1}$, $3d_0$, $3d_{\pm 1}$, $3d_{\pm 2}$, $4s$, $4p_0$, $4p_{\pm}1$ (sequential process 2 [see Eq. (6b)]), respectively. The full and dashed curves correspond to 41.8 eV and 44.9 photon energy, respectively.

We assume Gaussian profiles for both temporal and spatial shapes of the harmonic pulse, thus the intensity, $I(t;x,y,z)$ is expressed as

$$I(t;x,y,z) = I_0 \alpha(t) S(x,y,z), \tag{9}$$

where we define $\alpha(t)$ and $S(x,y,z)$ as

$$\alpha(t) \equiv \exp\{-\pi(t/\tau)^2\}, \tag{10}$$

$$S(x,y,z) \equiv \frac{w_0^2}{w^2(z)} \exp\left\{-2\frac{x^2+y^2}{w^2(z)}\right\}, \tag{11}$$

respectively. The time t is in the moving frame along the propagation axis z and the pulse width τ is determined such that the temporal profile satisfies $\int dt \alpha(t) = \tau$. The beam radius $w(z)$ depends on z as

$$w(z) = w_0\sqrt{1+(z/b)^2}, \tag{12}$$

where the confocal parameter b is obtained from w_0, M^2, and the wavelength of the harmonic beam λ with

$$b \equiv \frac{\pi w_0^2}{M^2 \lambda}. \tag{13}$$

Note that τ is almost the same as the FWHM pulse width.

A. Analytic solution

When neglecting depletion the rate equations can be solved analytically. Such a treatment allows us to emphasize the importance of the spatial integration or of the volume effect. This condition is well fulfilled in our experimental conditions as the probability for one-photon single ionization $I_0 \tau \sigma^+/(h\nu)$ and the N^{2+}/N^+ ratio, are both much smaller than 1. Within this approximation, the number of singly charged ions of can be expressed as

$$N^+ = n\int_{-\infty}^{\infty} dt \int_V d^3\mathbf{r} \frac{\sigma^+_{\mathrm{seq}_1}}{h\nu} I(t;x,y,z), \tag{14}$$

where n denotes the atomic density. The beam radius is much smaller than the radius of the TOF hole $(D/2)$; thus, the integration range for the transverse directions (x,y) is reasonably extended to $[-\infty,\infty]$ and it is equal to $[-D/2, D/2]$ for z. Straightforwardly we can express N^+ as

$$N^+ = n\frac{I_0\tau}{h\nu}\sigma^+_{\mathrm{seq}_1} V^+_{\mathrm{eff}}, \tag{15}$$

where we define the effective volume for one-photon single ionization as

$$V^+_{\mathrm{eff}} \equiv \frac{\pi w_0^2}{2} D. \tag{16}$$

The number of He^{2+} ions via the direct channel N^{2+}_{dir} and the sequential channels $N^{2+}_{\mathrm{seq}_1}$ and $N^{2+}_{\mathrm{seq}_2}$, can be computed as

$$N^{2+}_{\mathrm{dir}} = n\sigma^{2+}_{\mathrm{dir}} \int_{-\infty}^{\infty} dt \int_V d^3\mathbf{r} \frac{I^2(t;x,y,z)}{(h\nu)^2} = n\left(\frac{I_0\tau}{h\nu}\right)^2 \frac{\sigma^{2+}_{\mathrm{dir}}}{\tau} V^{2+}_{\mathrm{dir}} \tag{17}$$

and

$$N^{2+}_{\mathrm{seq}_1} = n\sigma^+_{\mathrm{seq}_1}\sigma^{2+}_{\mathrm{seq}_1} \int_{-\infty}^{\infty} dt_1 \int_{-\infty}^{\infty} dt_2 \int_V d^3\mathbf{r} \frac{I(t_1;x,y,z)}{h\nu} \times \theta(t_2-t_1)\frac{I^2(t_2;x,y,z)}{(h\nu)^2} = n\frac{I_0\tau}{h\nu}\sigma^+_{\mathrm{seq}_1}\left(\frac{I_0\tau}{h\nu}\right)^2 \frac{\sigma^{2+}_{\mathrm{seq}_1}}{\tau} V^{2+}_{\mathrm{seq}}, \tag{18}$$

$$N^{2+}_{\mathrm{seq}_2} = n\frac{I_0\tau}{h\nu}\sigma^{2+}_{\mathrm{seq}_2}\left(\frac{I_0\tau}{h\nu}\right)^2 \frac{\sigma^+_{\mathrm{seq}_2}}{\tau} V^{2+}_{\mathrm{seq}}, \tag{19}$$

respectively. The Heaviside function $\theta(t_2-t_1)$ represents the causality that doubly charged ions cannot be created before singly charged ions in the sequential process. The effective volumes for these ion yields V^{2+}_{dir} and V^{2+}_{seq} can be written as

$$V^{2+}_{\mathrm{dir}} = \frac{\pi}{2\sqrt{2}} \tan^{-1}\left(\frac{D}{2b}\right) w_0^2 b \tag{20}$$

and

$$V^{2+}_{\mathrm{seq}} = \frac{\pi}{12\sqrt{2}}\left[\tan^{-1}\left(\frac{D}{2b}\right) + \frac{D/(2b)}{1+\{D/(2b)\}^2}\right] w_0^2 b, \tag{21}$$

respectively. The total ion yield of He^{2+} is the sum of N^{2+}_{dir}, $N^{2+}_{\mathrm{seq}_1}$, and $N^{2+}_{\mathrm{seq}_2}$. Thus, the ratio of the He^{2+} yield to the He^+ yield can be expressed as

$$\frac{N^{2+}}{N^{+}} = \frac{\Gamma^{+}_{\mathrm{seq}_1}}{(\sigma^{+}_{\mathrm{seq}_1})^2}\left\{\sigma^{2+}_{\mathrm{dir}}\left(\frac{V^{2+}_{\mathrm{dir}}}{V^{+}_{\mathrm{eff}}}\right) + \Gamma^{+}_{\mathrm{seq}_1}\tau\left[\sigma^{2+}_{\mathrm{seq}_1}\left(\frac{V^{2+}_{\mathrm{seq}}}{V^{+}_{\mathrm{eff}}}\right) + \sigma^{2+}_{\mathrm{seq}_2}\frac{\sigma^{+}_{\mathrm{seq}_2}}{\sigma^{+}_{\mathrm{seq}_1}}\left(\frac{V^{2+}_{\mathrm{seq}}}{V^{+}_{\mathrm{eff}}}\right)\right]\right\}, \tag{22}$$

where $\Gamma^{+}_{\mathrm{seq}_1}$ the one-photon single ionization rate of He

$$\Gamma^{+}_{\mathrm{seq}_1} \equiv \frac{I_0}{h\nu}\sigma^{+}_{\mathrm{seq}_1}. \tag{23}$$

The first term in the square brackets in Eq. (22) originates from the TPDI process, whereas the second and the third terms come from the sequential processes. Hence, the competition of these two processes are determined not only by the ratio of $\sigma^{2+}_{\mathrm{dir}}$ to $\sigma^{2+}_{\mathrm{seq}}$, but also by the ratio of V^{2+}_{dir} to V^{2+}_{seq}.

By substituting the beam parameters described in Sec. III, we get that $\Gamma^{+}_{\mathrm{seq}_1}\tau V^{2+}_{\mathrm{seq}_1}/V^{2+}_{\mathrm{dir}}$ is only ~ 0.06. So the sequential channel will become the dominant process only if $\sigma^{2+}_{\mathrm{seq}_1}$ exceeds $\sigma^{2+}_{\mathrm{dir}}$ by a factor larger than $0.06^{-1} \simeq 17$. Following the theoretical predictions, the direct channel dominates the first sequential channel as this condition is not fulfilled with any of computed TPDI cross sections. A similar conclusion holds for the second sequential channel.

B. Numerical estimation

Because it is not possible to experimentally disentangle the contribution of the direct and sequential double ionization yields, raw experimental data have to be interpreted by means of a theoretical model. In other words, the estimation of the TPDI cross section requires to estimate the contributions of the sequential channels. In the present work we solve the rate equations [see Eqs. (8)] and average the computed probability over the spatial laser profile. In practice we tune the TPDI cross section in order to reproduce the experimental He^{2+} to He^{+} yield ratio. In order to get a lower bound of the cross section we use the minimum estimated ion ratio (4.4×10^{-5}). As it is very hard to accurately measure the beam waist and the pulse energy, we repeat the TPDI cross section estimation for a range of beam waists and pulse energies. The result is plotted in Fig. 13. It is estimated that the laser beam cannot be smaller than 1.55 μm and the pulse energy does not exceed 24 nJ. The point in Fig. 13 corresponds to this minimum beam size and this maximum pulse energy. As such the corresponding cross section ($\sigma_{\mathrm{min}} = 0.59\times10^{-52}$ cm^4 s) has to be interpreted as a lower bound of the TPDI cross section $\sigma_{\mathrm{TPDI}} \geqslant 0.59\times10^{-52}$ cm^4 s, because a smaller beam or a larger energy would result in a lower cross section. The comparison with theoretical predictions is plotted in Fig. 14.

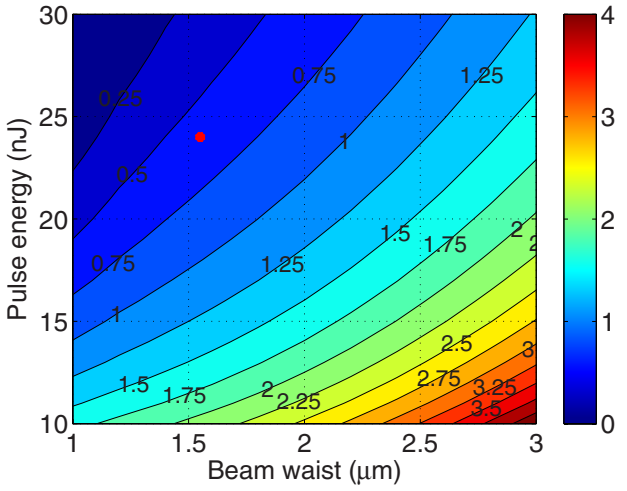

FIG. 13. (Color online) TPDI cross section from N^{2+}/N^{+} ratio (4.4×10^{-5}). The units are 10^{-52} cm^4 s.

The present lower bound is close but higher than a bunch of curves that correspond to cross sections computed with different time-dependent and time-independent approaches. There are actually five time-dependent approaches. The convergent close coupling result of Ivanov *et al.* [6], the close-coupling approach of Hu *et al.* [5] in which the time propagation is performed on a grid and the final wavepacket projected, a few cycles after the end of the pulse, on a product of two Coulomb functions. A similar method has been used recently by Feist *et al.* [11]. The two other time-dependent approaches are spectral methods that consist of expanding the total wave packet on square integrable functions: *B*-splines in the case of Laulan and Bachau [3] and Coulomb Sturmians in our case. The corresponding curves in Fig. 14 have been obtained by projecting the final wavepackets on a product of two Coulomb functions. Note the perfect agreement between Laulan's results, Feist's results for the same pulse duration and ours. The three time-independent approaches are the *R*-matrix Floquet method of Feng and van der Hart [4], the exterior complex scaling (ECF) method by Horner *et al.* [8], and the recent result of Shakeshaft [10]. As clearly stated in Feng *et al.* and Shakeshaft papers it is not clear whether their results have fully converged. Horner *et al.* state that their calculations are essentially exact [8]. Here we prefer to be more cautious. Let us stress that the strong effect due to the final state correlation we observe is also present in the calculations of Nikolopoulos *et al.* [9]. These results are the two curves with the highest cross sections in Fig. 14 (filled red circles and filled blue squares). Furthermore although the compatibility of the experimental data with the bunch of theoretical results requires experimental parameters that look unlikely, the small deviation prevents to draw definite conclusions about the different theoretical predictions in general and about the role of electron-electron correlations in the output channel in particular.

At 41.8 eV the contribution of the sequential channels is not negligible as illustrated in Fig. 15. It is reasonable to assume that the cross sections of the first sequential channel [see process (6a)] are well estimated. On the contrary, the resonant behavior of the TPSI cross section computed in Refs. [4,10] is not well understood. However, since it is the result of the lowest order of perturbation theory, it is reasonable to consider this data as an upper bound of the actual cross section. Figure 15 demonstrates that this upper bound results in an underestimation of the TPDI cross section that it limited and does not exceed 25%.

An interesting contribution has been recently submitted by Sorokin and collaborators [2]. They notably studied the

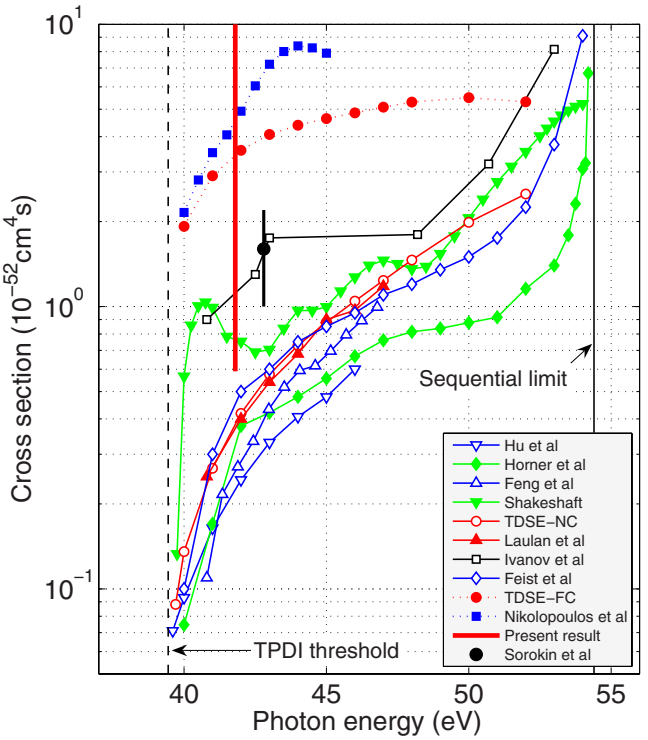

FIG. 14. (Color online) TPDI cross section. The results of Laulan *et al.* [3] (filled red triangles up), Piraux *et al.* [26] (open red circles), Hu *et al.* [5] (open blue triangles down), Ivanov *et al.* [6] (open black squares), Feist *et al.* [11] (open blue diamonds), Foumouo *et al.* [7] (filled red circles), Nikolopoulos *et al.* [9] (filled blue squares) are obtained with a time-dependent approach. Those of Feng *et al.* [4] (open blue triangles up), Hörner *et al.* [8] (filled green diamond), Shakeshaft [10] (filled green triangles down) are the theoretical predictions of time-independent models. Experimental results from Sorokin *et al.* [2]: open black circle. Present estimation: vertical red thick line. The lower bound corresponds to the bottom of the line.

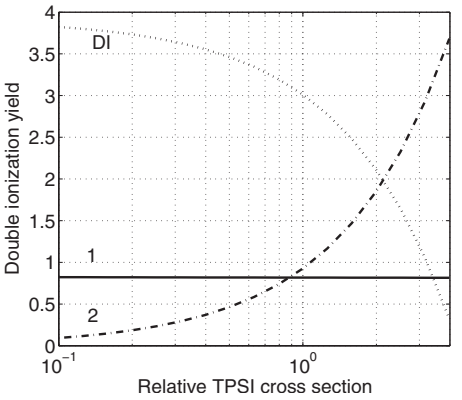

FIG. 15. Two-photon double ionization yield against the two-photon single ionization cross section. The TPSI cross section has been normalized to the cross section used in the present contribution. The dotted line (DI label), the solid line (1 label), and the dot-dashed line (2 label) are TPDI yield, the sequential 1 yield and the sequential 2 yield, respectively.

direct two-photon double ionization of helium with 42.8 eV photons. From the He^{2+} to He^{+} yield ratio they estimated the TPDI cross section to be $(1.6 \pm 0.6) \times 10^{-52}$ cm^4 s. It is worth noting that the experimental estimation depends on the spatial and temporal profiles chosen for the analysis of the experimental data. More precisely the section would have to be multiplied by a factor $2\sqrt{2}$ if Gaussian spatial and temporal profiles would have been used in place of square profiles.

V. CONCLUSIONS

We have presented an experimental determination of a lower bound of the two-photon double ionization cross section of helium. The photons have an energy of 41.8 eV and are produced as the 27th harmonic of an Ti:sapphire laser. The ratio of the number of the double charged ions to the number of single charged ions has been measured. The cross section is extracted from the raw data by averaging the ionization probability over the time and the spatial profiles of the laser beam and by estimating the ionization yields of the sequential channels. We have shown that at a photon energy of 41.8 eV, the sequential processes contribute significantly to the double ionization yield. By taking into account their contributions and by carefully analyzing various experimental parameters, we have been able to derive a lower bound of the TPDI cross section. However, its value does not allow one to draw definite conclusions regarding the validity of the different theoretical approaches, in general, and the impact of the electron-electron correlation in the output channel in particular.

ACKNOWLEDGMENTS

We wish to acknowledge R. Shakeshaft for providing theoretical results before publication and for many suggestions. We also thank P. Lambropoulos for many interesting discussions. This work is supported by the FNRS (Fonds National de la Recherche Scientifique) through the FRFC Project No. 2.4592.07. The experimental research is supported by the MEXT (Ministry of Education, Culture, Sports, Science, and Technology) in Japan through a Grant for Extreme Photonics Research. The authors thank the Université catholique de Louvain for providing them with access to the supercomputer of the CISM (Centre de Calcul Intensif et Stockage de Masse) which is supported by the FNRS (Fonds National de la Recherche Scientifique) through the FNRC (Fonds de la Recherche Fondamentale et Collective) Project No. 2.4556.99, "Simulations Numériques et traitement de données."

[1] H. Hasegawa, E. J. Takahashi, Y. Nabekawa, K. L. Ishikawa, and K. Midorikawa, Phys. Rev. A **71**, 023407 (2005).
[2] A. A. Sorokin, M. Wellhöfer, S. V. Bobashev, K. Tiedtke, and M. Richter, Phys. Rev. A **75**, 051402(R) (2007).
[3] S. Laulan and H. Bachau, in *International Conference on Electron and Photon Impact Ionization and Related Topics*, edited by L. U. Ancarani, IOP Conf. Ser. No. 172 (Institute of Physics, Bristol, 2003), p. 109.
[4] L. Feng and B. H. W. van der Hart, J. Phys. B **36**, L1 (2003).
[5] S. X. Hu, J. Colgan, and L. A. Collins, J. Phys. B **38**, L35 (2005).
[6] I. Ivanov and A. Kheifets, J. Phys. B **41**, 095002 (2008).
[7] E. Foumouo, G. L. Kamta, G. Edah, and B. Piraux, Phys. Rev. A **74**, 063409 (2006).
[8] D. A. Horner, F. Morales, T. N. Rescigno, F. Martin, and C. W. McCurdy, Phys. Rev. A **76**, 030701(R) (2007).
[9] L. A. A. Nikolopoulos and P. Lambropoulos, J. Phys. B **40**, 1347 (2007).
[10] R. Shakeshaft, Phys. Rev. A **76**, 063405 (2007).
[11] J. Feist, S. Nagele, R. Pazourek, E. Persson, B. I. Schneider, L. A. Collins, and J. Burgdörfer, Phys. Rev. A **77**, 043420 (2008).
[12] E. Foumouo, P. Antoine, B. Piraux, L. Malegat, H. Bachau, and R. Shakeshaft, J. Phys. B **14**, 051001 (2008).
[13] L. A. A. Nikolopoulos and P. Lambropoulos, J. Phys. B **39**, 883 (2006).
[14] T. Nakajima and L. A. A. Nikolopoulos, Phys. Rev. A **66**, 041402(R) (2002).
[15] P. Lambropoulos (private communications).
[16] H. Hasegawa, E. J. Takahashi, Y. Nabekawa, and K. Midorikawa, Laser Phys. **15**, 812 (2005).
[17] Y. Nabekawa, H. Hasegawa, E. J. Takahashi, and K. Midorikawa, Phys. Rev. Lett. **94**, 043001 (2005).
[18] E. Takahashi, Y. Nabekawa, T. Otsuka, M. Obara, and K. Midorikawa, Phys. Rev. A **66**, 021802(R) (2002).
[19] E. J. Takahashi, Y. Nabekawa, H. Mashiko, H. Hasegawa, A. Suda, and K. Midorikawa, IEEE J. Sel. Top. Quantum Electron. **10**, 1315 (2004).
[20] E. J. Takahashi, H. Hasegawa, Y. Nabekawa, and K. Midorikawa, Opt. Lett. **29**, 507 (2004).
[21] H. Mashiko, A. Suda, and K. Midorikawa, Opt. Lett. **29**, 1927 (2004).
[22] L. A. A. Nikolopoulos and P. Lambropoulos, Phys. Rev. Lett. **97**, 169301 (2006).
[23] J. A. R. Samson, Z. X. He, L. Yin, and G. N. Haddad, J. Phys. B **27**, 887 (1994).
[24] F. T. Chan and C. L. Tang, Phys. Rev. **185**, 42 (1969).
[25] R. Shakeshaft (private communication).
[26] B. Piraux, J. Bauer, S. Laulan, and H. Bachau, Eur. Phys. J. D **26**, 7 (2003).